International Journal of Applied and Physical Sciences
volume 7 pp. 27-35 doi: https://dx.doi.org/10.20469/ijaps.7.50004

The Pyrolysis Characteristics and Thermogravimetric Kinetic Analysis of the Pyrolysis of CIGS Nanocrystals

Hong-Ming Lin*
Institute of Mineral Resources Engineering,
National Taipei University of Technology,
Taipei, Taiwan

Kai-Chungand Hsu
Institute of Mineral Resources Engineering,
National Taipei University of Technology,
Taipei, Taiwan

Jyh-Herng Chen
Institute of Mineral Resources Engineering,
National Taipei University of Technology,
Taipei, Taiwan

Abstract: A kinetic of the thermo-oxidative decomposition of CIGS nanoparticles is investigated with a thermogravimetric analyzer with non-isothermal methods. The weight loss was measured by TGA in the air atmosphere. The samples were heated over a range of temperatures from 300 K to 1,100 K with three different heating rates of 2, 5, and 10°C min-$^{-1}$. The results obtained from the thermal decomposition process indicate that there are two stages of thermal decomposition in the temperature range. The binary/ternary selenide is formed in the first stage. The invariant activation energy and frequency factor (LNA) in the first stage are 143.76 kJ/mol and 20.93 1/sec, respectively. In the second stage, the selenide begins to be oxidized to form a metal oxide. The invariant activation energy and frequency factor (LNA) in the second stage are 222.81 kJ/mol and 25.90 1/sec, respectively. The determined most probable g(α) functions are g(α) = (1-α)$^{-2}$-1 for both stages.

Keywords: *Thermal decomposition, $CuIn_xGa_{1-x}Se^{-1}$, chalcopyrite, nanoparticles, thermogravimetric analyzer*

Received: 08 August 2021; ***Accepted:*** 15 October 2021; ***Published:*** 05 December 2021

I. INTRODUCTION

There is a wide variety of materials that exhibit photovoltaic effects. According to the material properties, they can be roughly divided into silica-based material, III-V or II-VI group semiconductor material, and organic conductive polymer material. Among them, the I-III-VI group quaternary semiconductor material composed of $CuIn_xGa_{1-x}Se^{-1}$ CIGS has gradually stood out from Thin-Film Solar Cells (TFSC) due to its high light absorption coefficient (α = 105 cm^{-1}), wide energy level range (1.02 – 1.68 eV), direct band gap semiconductor, high stability, and other advantages. At present, the best photoelectric conversion efficiency of CIGS solar cells fabricated using vacuum process technology is 19.0% – 21.7% [1, 2, 3, 4]. Recently, thermal analysis kinetics has been extensively developed. It is widely applied in research fields, such as chemical engineering, material synthesis, ceramics' thermal stability, and photo-catalyst degradation [5]. The results of thermal analysis kinetics can also be used as an important index for industrial production evaluation.

The technology uses variable temperature conditions to st. The kinetic process of the reaction of substances and calculate the kinetic triplet of the reaction, which is respectively the apparent activation energy E_a, frequency factor, or pre-exponential factor A and reaction model. At

*Correspondence concerning this article should be addressed to Hong-Ming Lin, Institute of Mineral Resources Engineering, National Taipei University of Technology, Taipei, Taiwan. E-mail: 3f10871@ntut.edu.tw

present, thermal analysis kinetics is widely used in synthesizing organic and inorganic materials and studying thermal–oxidative decomposition.

In this study, the dynamic and thermal analysis of the thermal decomposition of CIGS with chalcopyrite structure in the air was performed using a thermal gravimetric analyzer in non-isothermal mode, and the changes in the crystal phase at different temperatures were discussed.

II. TEST METHODS

A. *Nanopowder Synthesis of CIGS with Chalcopyrite Structure*

The CIGS particles with In/(In+Ga) ratio of 0.7 synthesized by the one-pot solvothermal method was studied. The reference to the synthetic method is made to the literature of Zhang Xu et al. [6]: simultaneously add 1 mmole $Cu(acac)_2$, 2 mmole selenium powder, 0.7 mmol $In(acac)_3$, and 0.3 mmol $Ga(acac)_3$ into the reaction bulb containing an appropriate amount of melamine at room temperature, and place the reaction bulb on the stirrer heater. After 30 min of evacuation by a vacuum pump, nitrogen was injected for 30 min to remove steam and oxygen in the reaction environment. Next, thoroughly mix the reactants to avoid the influence of oxide and impurity in the reaction process or product. Repeat the step thrice, raise the temperature to 250°C in a low-pressure environment, and then lower the temperature to 60°C after holding the temperature for 4 h. After repeated washing with ethanol–toluene and vacuum drying, the CIGS nanopowder with In/(In+Ga) ratio of 0.7 were obtained.

B. *Thermogravimetric Analysis Test*

Thermal gravimetric analysis (TGA, TA Q50) was used for the thermogravimetric analysis of samples. The CIGS powder with chalcopyrite structure was placed in a platinum crucible and heated from room temperature to 1100°C at different heating rates of 2, 5, and 10°C/min in air.

C. *Thermal Decomposition Kinetics*

The non-isothermal kinetic method is commonly used at present [7]. Its kinetic differential equation can be generally expressed as follows:

$$\frac{d\alpha}{dt} = kf(\alpha) \tag{1}$$

In addition, the relationship between reaction rate constant k and temperature can be obtained by the Arrhenius formula:

$$k = A\exp\left(\frac{-E_\alpha}{RT}\right) \tag{2}$$

Wherein is the conversion rate; E_a is the apparent activation energy (J/mol); A is the frequency factor (pre-exponential factor) (< 1 / sec); T is the reaction temperature (K) corresponding to the conversion rate. Substituting equation 1 into equation 2

$$\frac{d\alpha}{dt} = \mathrm{Aexp}\left(\frac{-E_{\mathrm{at}}}{RT}\right) f(\alpha) \tag{3}$$

For the non-isothermal method, equation 3 is rearranged and integrated to obtain:

$$\mathrm{g}(\alpha) = \int_{T_0}^{T}\left(\frac{A}{R_h}\right)\exp\left(\frac{-E_a}{RT}\right)dT \approx \int_{0}^{T}\left(\frac{A}{R_h}\right)\exp\left(\frac{-E_a}{RT}\right)dT = \left(\frac{AE_a}{R_hR}\right)g(x) \tag{4}$$

In equation 4, when the integrated value of the lower limit of integral T_0 approaches 0, the lower limit of integral may be replaced by 0. g(x) is referred to as the integral temperature approximation.

D. *Multi-heating Rate Method*

The multi-heating rate method refers to the kinetic analysis performed according to several thermal analysis curves measured at different heating rates [8]. Since most multi-heating rate methods use the same conversion rate (α) data on several thermal analysis curves for kinetics processing, the multi-heating rate method is also called the iso-conversion method. In this study, Kissinger Akahira Sunose (KAS) and Flynn Wall Ozawa (FWO) is used for analysis, and their respective linear equations are as shown in equation 5 and 6:

$$\ln\left(\frac{R_h}{T^2}\right) = \ln\frac{AR}{g(a)E_a} - \frac{E_a}{RT} \tag{5}$$

$$\ln(R_h) = \ln\frac{0.0048AE_a}{g(a)R} - 1.052\frac{E_a}{RT} \tag{6}$$

III. RESULTS AND DISCUSSION

A. *Thermogravimetric Loss of CIGS with Chalcopyrite Structure Under different Heating Rates*

Fig. 1 shows the thermogravimetric loss curve for thermal–oxidative decomposition of CIGS with chalcopyrite structure in the air at different heating rates. The non-isothermal thermal–oxidative decomposition of CIGS with chalcopyrite structure can be roughly divided into three thermogravimetric loss processes; taking the heating rate of 2°C/min as an example, namely the room temperature to 558 K (the first thermogravimetric loss process), 558 K to 660 K (the second thermogravimetric loss process) and 727 K to 886 K (the third thermogravimetric loss process). By comparing the thermogravimetric curves under different heating rates, it can be seen that the thermogravimetric loss of each stage at the same temperature decreases with the increase in the heating rate. Table 1 shows the thermal–oxidative decomposition loss rate corresponding to a change in the thermogravimetric loss at each heating rate. In this study, the total weight at each stage was considered as 1.0 based on the thermogravimetric change at each heating rate, and the decomposition rate (α) was compared with the weight loss at each stage.

In the first thermogravimetric loss process, the surface adsorbed water and the oleylamine protective agent of the sample were lost. However, the relative content was small, and there was no noticeable effect on the crystal phase change of the sample.

B. *XRD Crystal Phase Analysis of CIGS with Chalcopyrite Structure in the Air Under Different Thermal–oxidative Decomposition Temperature*

To understand each thermal–oxidative decomposition reaction of CIGS with chalcopyrite structure in air, XRD crystal phase analysis (heating rate is 5°C/min) was performed on the thermal–oxidative decomposition products in the air at different TGA reaction temperatures (400°C, 600°C, 700°C, 800°C, and 1,000°C).

Fig. 2 shows the XRD crystal phase analysis of CIGS with chalcopyrite structure in the air under different reaction temperatures. When the sample reacts at 400 K, its diffraction peak shows the crystal plane diffraction peak of chalcopyrite structure $CuIn_{0.7}Ga_{0.3}Se_2$ (PDF # 35-1102), which indicates that in the first thermogravimetric loss process, the weight loss of the sample was not caused by the thermal–oxidative decomposition of the CIGS with chalcopyrite structure. So, it can be confirmed that the first weight loss process of TGA was caused by the evaporation and decomposition of surface adsorbed water and oleylamine.

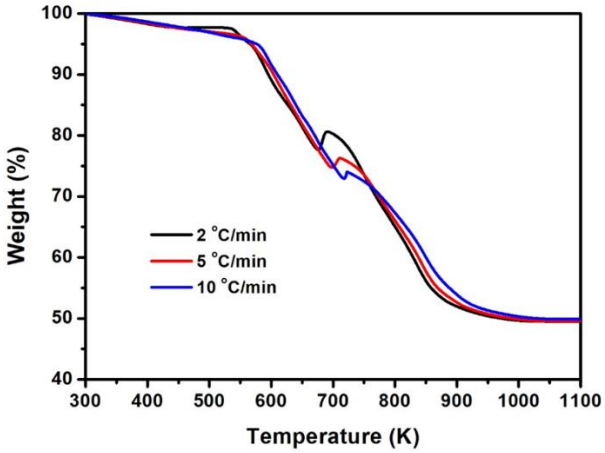

Fig. 1. Thermogravimetric loss curve of chalcopyrite structure in air under different heating rates (2, 5, and 10°C/min)

The crystal phase structure is different from that of chalcopyrite as the temperature is increased to 600 K, which is composed of $CuIn_{0.7}Ga_{0.3}Se_2$ (PDF # 35-1102), CuSe (PDF # 86-1240), and In_2O_3 (PDF # 71-2195). This indicates that CIGS with a chalcopyrite structure begins thermal–oxidative decomposition with the increase in temperature. However, in contrast to the result of the TGA curve, the second thermogravimetric loss process is incomplete. Moreover, except for CuSe and In_2O_3 produced in the thermal–oxidative decomposition, part of the CIGS of the chalcopyrite structure remains. Therefore, in the second thermogravimetric loss process for CIGS with chalcopyrite structure in air, metal selenide is mainly produced in the thermal–oxidative decomposition of CIGS with chalcopyrite structure.

When the temperature reaches 700 K, its crystal phase structure is composed of $Cu_2O(SeO_3)$ (PDF # 77-2327), Cu_2Se (PDF # 88-2044), and In_2O_3 (PDF # 71-2195). Compared with the results in Fig. 1, there is a substantial weight increase at this temperature, and it can be judged that it is owing to the production of $Cu_2O(SeO_3)$. When the temperature reaches 800 K later, its crystal phase structure is composed of $CuInGaO_4$ (PDF # 73-1866), CuO (PDF # 48-1548), and In_2O_3 (PDF # 71-2195); therefore, in the second thermogravimetric loss process for CIGS with chalcopyrite structure in air, metallic oxides is mainly produced.

Moreover, when the temperature reaches 1,000 K, its crystal phase structure is composed of $CuInGaO_4$ (PDF # 73-1866), CuO (PDF # 48-1548), and In_2O_3 (PDF # 71-2195), and the diffraction peak intensity of each crystal phase increases significantly as the temperature increases.

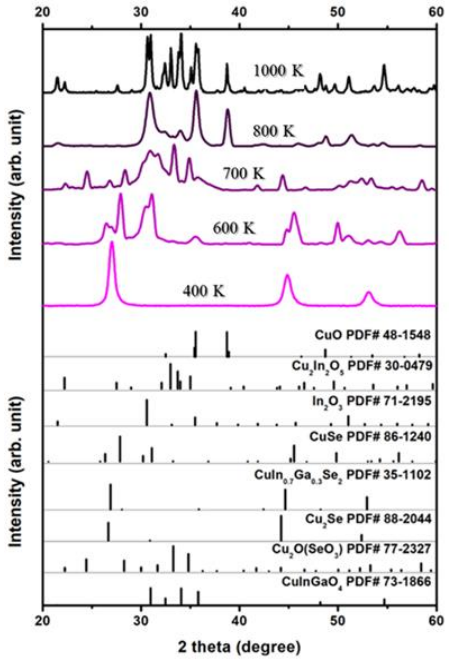

Fig. 2. XRD crystal phase analysis of products under different temperatures for CIGS with chalcopyrite structure in air (5°C/min)

C. *Relationship Between Apparent Activation Energy and Conversion Rate for Thermal–oxidative Decomposition of CIGS with Chalcopyrite Structure*

In this study, the kinetic triplet of thermal–oxidative decomposition of CIGS with chalcopyrite structure was studied using the isoconversion method, and the apparent activation energy of thermal–oxidative decomposition under different conversion rates was calculated using FWO and KAS methods, respectively.

1) Stage I: Fig. 3 and 4 are the linear equation relationship diagrams of Stage I thermal–oxidative decomposition of CIGS with chalcopyrite structure using the isoconversion method. The results show evident linear relations under different thermal–oxidative decomposition rates. When the thermal–oxidative decomposition rate ranges from 0.2–0.8, and the R^2 values of different methods generally range from 0.9999 to 0.9976, the apparent activation energies calculated by FWO and KAS methods are in the range of 152.03–156.28 and 150.11–153.33 kJ/mol, respectively under different thermal–oxidative decomposition rate. The results in apparent activation energies by each method are similar. In addition, the apparent activation energy calculated by each method basically remains constant within the range of the thermal–oxidative decomposition rate, indicating that the kinetic parameters do not vary depending on the thermal–oxidative decomposition rate. In other words, the Stage I thermal–oxidative decomposition of CIGS with chalcopyrite structure is a single-step reaction and can be described using a single kinetic parameter.

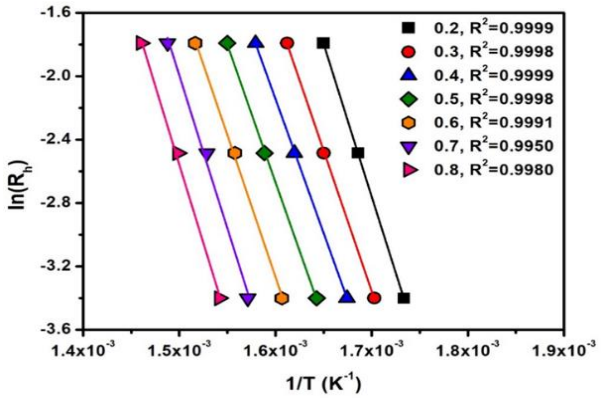

Fig. 3. Iso-conversion method for stage i thermal-oxidative decomposition of CIGS with chalcopyrite structure in air - FWO linear relation diagram

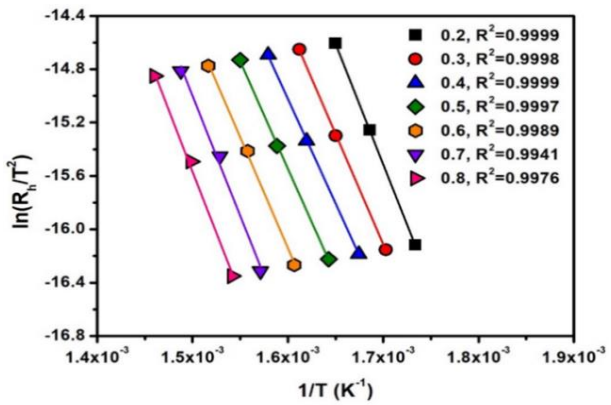

Fig. 4. Iso-conversion method for stage i thermal-oxidative decomposition of CIGS with chalcopyrite structure in air - KAS linear relation diagram

The average apparent activation energies calculated by FWO and KAS methods are 144.64 and 141.73 kJ/mol, respectively.

2) Stage II: Fig. 5 and 6 are the linear equation relationship diagrams of Stage II thermal–oxidative decomposition of CIGS with chalcopyrite structure using the isoconversion method. First, the results of different methods also show obvious linear relations under different thermal–oxidative decomposition rates. For example, when the thermal–oxidative decomposition rate ranges from 0.2 - 0.8, and the R^2 values of different methods generally range from 0.9999 to 0.9585, the apparent activation energies calculated by FWO and KAS methods are in the range of 184.28–279.96 and 180.85–280.36 kJ/mol, respectively under different thermal–oxidative decomposition rate. The results in apparent activation energies by each method are similar. It indicates that the kinetic parameters of Stage II thermal–oxidative decomposition do not vary depending on the thermal–oxidative decomposition rate, so it can be confirmed that the Stage II

thermal–oxidative decomposition of chalcopyrite structure is also a single-step reaction and can be described using a single kinetic parameter.

The average apparent activation energies calculated by FWO and KAS methods are 226.51 and 224.69 kJ/mol, respectively.

TABLE 1
SUMMARY OF APPARENT ACTIVATION ENERGIES AND FREQUENCY FACTORS OF FUNCTION CALCULATION UNDER DIFFERENT REACTION MODES FOR ANALYSIS OF STAGE I THERMAL–OXIDATIVE DECOMPOSITION OF CIGS WITH CHALCOPYRITE STRUCTURE BY COATS–REDFERN METHOD

	(2°/min			(5°/min			10°/min			Avg. Ea (kJ/mol)	Avg. lnA(1/sec)
Model	E_a(kJ/mol)	lnA(1/sec)	R^2	E_a(kJ/mol)	lnA(1/sec)	R^2	E_a(kJ/mol)	lnA(1/sec)	R^2		
F3/2	86.94	9.25	0.9892	91.45	10.50	0.9981	89.48	10.33	0.9979	89.29	10.03
F2	104.38	13.79	0.9938	109.52	15.05	0.9979	107.17	14.72	0.9959	107.02	14.52
F3	144.62	23.23	0.9922	151.19	24.53	0.9894	147.91	23.83	0.9846	147.91	23.86
A1, F1	71.52	6.50	0.9780	75.45	7.74	0.9927	73.83	7.70	0.9948	73.60	7.31
A2/3	112.36	14.79	0.9801	118.40	16.19	0.9935	116.11	15.83	0.9954	115.62	15.60
A3/4	98.75	12.05	0.9796	104.08	13.39	0.9933	102.01	13.14	0.9952	101.62	12.86
A5/2	22.51	-4.06	0.9635	23.91	-3.01	0.9876	23.11	-2.66	0.9908	23.17	-3.24
A1/2	153.21	22.94	0.9810	161.35	24.50	0.9938	158.37	23.81	0.9956	157.64	23.75
A1/3	234.90	39.04	0.9819	247.26	40.92	0.9941	242.92	39.58	0.9958	241.69	39.85
A1/4	316.59	55.02	0.9823	333.16	57.22	0.9943	327.46	55.22	0.9960	325.73	55.82
D5	713.31	25.10	0.9881	182.21	26.68	0.9974	178.78	25.81	0.9979	178.10	25.86

TABLE 2
SUMMARY OF APPARENT ACTIVATION ENERGIES AND FREQUENCY FACTORS OF FUNCTION CALCULATION UNDER DIFFERENT REACTION MODES FOR ANALYSIS OF STAGE II THERMAL–OXIDATIVE DECOMPOSITION OF CIGS WITH CHALCOPYRITE STRUCTURE BY COATS–REDFERN METHOD

	(2°/min			(5°/min			10°/min			Avg. Ea (kJ/mol)	Avg. lnA(1/sec)
Model	E_a(kJ/mol)	lnA(1/sec)	R^2	E_a(kJ/mol)	lnA(1/sec)	R^2	E_a(kJ/mol)	lnA(1/sec)	R^2		
F3/2	97.53	6.40	0.9946	112.00	9.17	0.9969	115.58	10.01	0.9991	108.37	8.52
F2	117.06	10.44	0.9925	134.06	13.51	0.9934	138.42	14.39	0.9969	129.85	12.78
F3	162.08	18.74	0.9810	184.92	22.50	0.9803	191.06	23.47	0.9856	179.35	21.57
A1, F1	80.23	4.08	0.9913	92.44	6.59	0.9954	95.36	7.39	0.9963	89.34	6.02
A2/3	126.96	11.37	0.9923	145.45	14.63	0.9959	149.98	15.49	0.9967	140.80	13.83
A3/2	49.07	-0.97	0.9895	57.11	1.05	0.9945	58.95	1.81	0.9955	55.04	0.63
A3/4	111.38	8.96	0.9921	127.79	11.97	0.9958	131.78	12.81	0.9966	123.65	11.25
A5/2	24.14	-5.32	0.9838	28.84	-3.68	0.9919	29.82	-2.95	0.9931	27.60	-3.98
A2	33.49	-3.63	0.9871	39.44	-1.85	0.9934	40.74	-1.10	0.9945	37.89	-2.19
A3	17.91	-6.53	0.9792	21.77	-4.97	0.9899	22.54	-4.24	0.9913	20.74	-5.25
A4	10.12	-8.24	0.9624	12.94	-6.75	0.9833	13.43	-6.04	0.9853	12.16	-7.01
A1/2	173.70	18.52	0.9927	198.46	22.52	0.9961	204.60	23.45	0.9969	192.25	21.50
A1/3	267.16	32.62	0.9931	304.48	38.11	0.9963	313.85	39.17	0.9970	295.16	36.63
A1/4	360.64	46.59	0.9933	410.49	53.59	0.9964	423.08	54.76	0.9971	398.07	51.64
D5	196.26	20.12	0.9951	223.95	24.46	0.9974	230.96	25.43	0.9990	217.06	23.34

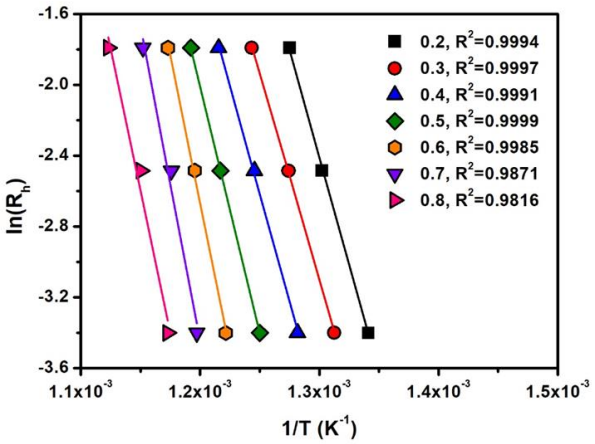

Fig. 5. Isoconversion method for stage ii thermal-oxidative decomposition of CIGS with chalcopyrite structure in air - FWO linear relation

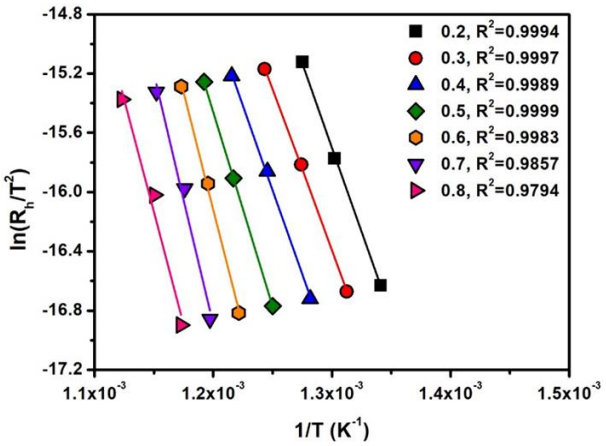

Fig. 6. Iso-conversion method for stage ii thermal-oxidative decomposition of CIGS with chalcopyrite structure in air - KAS linear relation

D. *Kinetic Model Study on Thermal–oxidative Decomposition of CIGS with Chalcopyrite Structure in the Air*

In this study, the Coats–Redfern method was used for analysis to accurately describe the kinetic process of thermal–oxidative decomposition of CIGS with chalcopyrite structure. The apparent activation energy, frequency factor, and dynamic model at various heating rates were analyzed using the linear matching coefficients of 39 common models. The basic formula of reaction using the Coats–Redfern method is as follows:

$$\frac{d\alpha}{dt} = \mathrm{A}\exp\left(\frac{-E_\alpha}{RT}\right) f(\alpha) \tag{7}$$

Where in α is conversion rate, t is reaction time (sec), A is frequency factor (1/sec), E_a is apparent activation energy (J/mol), T is the reaction temperature (K) corresponding to conversion rate, R is the ideal gas constant (8.314 J/mol·K); $f(\alpha)$ is the response mode function. For non-isothermal kinetics experiments, the heating rate R_h can be expressed as dT/dt, substituting it into equation 1; the following is obtained:

$$\frac{d\alpha}{dT} = \frac{1}{R_h}\frac{d\alpha}{dt} = \frac{A}{R_h}\exp\left(\frac{-E_{\mathrm{at}}}{RT}\right) f(\alpha) \tag{8}$$

Integrate equation 2 and take the logarithm, Coats–Redfern equation is obtained:

$$\int_0^\alpha \frac{d\alpha}{f(\alpha)} = \int_0^T \frac{A}{R_h}\exp\left(\frac{-E_a}{RT}\right) dT \tag{9}$$

In general, (1-2RT/E_a) $\approx$ 1; therefore, equation 4 can be simplified as follows:

$$\ln\left(\frac{g(\alpha)}{T^2}\right) = \ln\frac{AR}{R_h E_A}\left(1-\frac{2RT}{E_a}\right) - \frac{E_a}{RT} \tag{10}$$

In general, (1-2RT/E_a) $\approx$ 1; therefore, equation 4 can be simplified as follows:

$$\ln\left(\frac{g(\alpha)}{T^2}\right) = \ln\frac{AR}{R_h E_A} - \frac{E_a}{RT} \tag{11}$$

In the Coats–Redfern method, a common integral mode function is substituted into the equation, plotted against 1/T by $\ln\left(\frac{g(\alpha)}{\pi^2}\right)$, and performed linear matching. The activation energy E_a and the frequency constant A under each reaction mode function were obtained using the linear equation's slope $\left(\frac{-E_a}{RT}\right)$ and intercept $\left(\ln\frac{AR}{R_h E_Q}\right)$.

1) Stage I: As shown in Table 1, compared with the average apparent activation energy obtained by the KAS method (E_a = 141.73 kJ/mol), the reaction mode function of Stage I thermal–oxidative decomposition for CIGS with chalcopyrite structure is close to the F3 reaction mode g(α) = (1-α)$^{-2}$-1. In F3 reaction mode, the results in apparent activation energy at different heating rates of 2, 5, and 10°C/min are 144.62, 151.19, and 147.91 kJ/mol, respectively; LAN values are 23.23, 24.53, and 23.83 1/sec, respectively; and R^2 values are 0.9922, 0.9894 and 0.9846, respectively. The average apparent activation energy and average lnA in F3 reaction mode are 147.91 kJ/mol and 23.86 1/sec, respectively.

2) Stage II: As shown in Table 2, compared with the average apparent activation energy obtained by KAS method (E_a = 224.69 kJ/mol), the reaction mode function of Stage II thermal–oxidative decomposition for CIGS with chalcopyrite structure is close to the D5 reaction mode $g(\alpha) = \left[(1-\alpha)^{-\frac{1}{3}} - 1\right]^2$. In D5 reaction mode, the results in apparent activation energy at different heating rates of 2, 5, and 10°C/min are 196.26, 223.95, and 230.96 kJ/mol, respectively; lnA values are 20.12, 24.46, and 25.43 1/sec, respectively; and R^2 values are 0.9951, 0.9974 and 0.9990, respectively. The average apparent activation energy and average lnA in D5 reaction mode are 217.06 kJ/mol and 23.34 1/sec, respectively.

E. *Analysis of True Dynamic Parameters for Thermal–oxidative Decomposition of CIGS with Chalcopyrite Structure in the Air*

In theory, the kinetic triplet shall be a mutually independent variable. However, Gallagherh et al. [9] proposed the kinetic compensation effect, which suggests that in the same reaction of the same reactant under different reaction conditions, the corresponding frequency factor also increases or decreases as the activation energy increases or decreases. That is, there is a mutual compensation relationship between apparent activation energy and frequency factor, which are two kinetic parameters with opposite effects on the reaction rate, as shown in equation 6:

$$\ln A = b_{R_h} E_a + a_{R_h} \tag{12}$$

Wherein both a_{R_h} and b_{R_h} are kinetic compensation constants. The line fitted by the linear relation between apparent activation energy and frequency factor for each mode function obtained by the Coats–Redfern integral method at each heating rate will intersect at a point, which represents the apparent activation energy and frequency factor values corresponding to the real response mode,

namely the Invariant Kinetic Parameter (IKP) $E_{a,inv}$ and $\ln A_{inv}$ [10].

In fact, due to the influence of experimental conditions, these lines are difficult to intersect at a point instead of intersecting within a certain region. Therefore, in order to eliminate the influence of experimental conditions on $E_{a,inv}$, and $\ln A_{inv}$, the relational expression equation 3 can be derived from the relational expression of compensation effect equation 2 under different heating rates: according to the kinetic compensation parameters a_{R_h} and b_{R_h} obtained under different heating rates, the invariant kinetic parameters $E_{a,inv}$ and $\ln A_{inv}$ are calculated by the slope and intercept of the linear equation.

$$a_{R_h} = \ln A_{inv} - E_{a,inv} b_{R_h} \tag{13}$$

1) Stage I: Fig. 7 shows the linear compensation relation of kinetic parameters for Stage I thermal–oxidative decomposition of CIGS with chalcopyrite structure at each heating rate. The table in the figure is the summary of the resulting kinetic compensation parameters. The true kinetic parameters $E_{a,inv}$,and $\ln A_{inv}$ calculated by the slope and intercept in Fig. 7 are 143.76 kJ/mol and 20.93 1/sec, respectively, which is also similar to those calculated by the isoconversion method. Compared with the average apparent activation energies and frequency factors listed in Table 1, it can be seen that using the results obtained by the IKP method, the reaction mode function of Stage I thermal–oxidative decomposition of CIGS with chalcopyrite structure is also applied to the F3 mode.

Therefore, the Stage I thermal–oxidative decomposition of CIGS with chalcopyrite structure is the random nucleation of three epipoles on one separate particle [11].

2) Stage II: Fig. 8 shows the linear compensation relation of kinetic parameters for Stage II thermal–oxidative decomposition of CIGS with chalcopyrite structure at each heating rate. The table in the figure summarizes the resulting kinetic compensation parameters. The true kinetic parameters $E_{a,inv}$, and $\ln A_{inv}$ calculated by the slope and intercept in Fig. 8 are 222.81 kJ/mol and 25.90 1/sec, respectively, which is also similar to those calculated by the iso-conversion method. Comparing the average apparent activation energies and frequency factors listed in Table 2, it can be seen that by using the results obtained by the IKP method, the reaction mode function of Stage II thermal–oxidative decomposition of CIGS with chalcopyrite structure is also applied to the F1 mode.

Therefore, the Stage II thermal–oxidative decomposition of CIGS with chalcopyrite structure is the random nucleation of three epipoles on one separate particle [11].

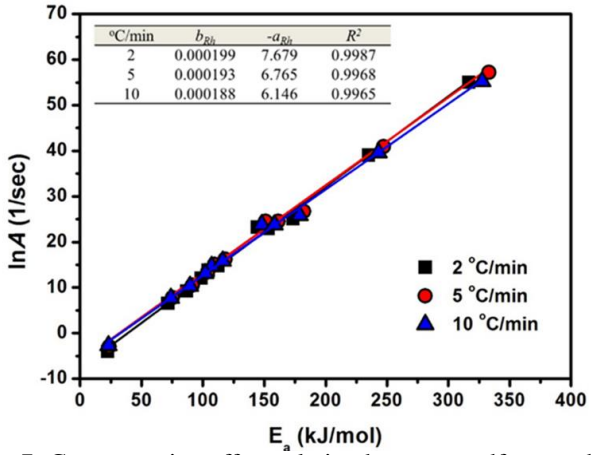

Fig. 7. Compensation effect relation by coats-redfern method for stage i thermal-oxidative decomposition of CIGS with chalcopyrite structure

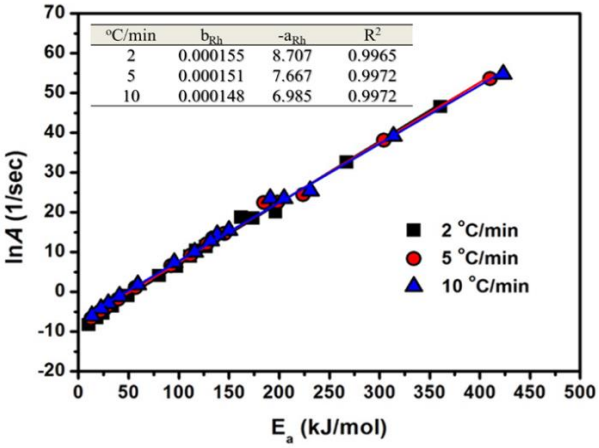

Fig. 8. Compensation effect relation by coats-redfern method for stage ii thermal-oxidative decomposition of CIGS with chalcopyrite structure

F. Thermodynamic Activation Parameter Calculation for Thermal–oxidative Decomposition of CIGS with Chalcopyrite Structure in the Air

Table 3 shows the changes in thermodynamic activation parameters calculated by the average apparent activation energy at a different heating rate of each thermal–oxidative decomposition temperature obtained by the KAS method.

The results show that the reaction activation enthalpy and entropy almost overlap in Stage I and Stage II thermal–oxidative decompositions at each heating rate, indicating the influence of heating rate on activation enthalpy and activation entropy is negligible. The reaction activation enthalpies of the two stages of thermal–oxidative decomposition under each heating rate are positive, indicating that the Stage I and Stage II thermal–oxidative decompositions of CIGS with chalcopyrite structure are endothermic reactions; the activation entropies of

Stage I and Stage II thermal–oxidative decompositions of CIGS with chalcopyrite structure are negative, which also indicates that the activated complex produced by the two-stage reactions has a more ordered structure than the reactant [12]. The average activation entropies of Stage I and Stage II thermal–oxidative decompositions of CIGS with chalcopyrite structure are 0.085 and 0.046 kJ/K·mol, respectively, indicating that the Stage I and Stage II thermal–oxidative decompositions of CIGS with chalcopyrite structure are slow reactions [13]; the activation free energies of Stage I and Stage II thermal–oxidative decompositions of CIGS with chalcopyrite structure are positive, indicating that both stages are non-spontaneous reactions. In addition, the calculated results also show that the reaction apparent activation energies of Stage I and Stage II thermal–oxidative decompositions of CIGS with chalcopyrite structure are similar to the activation enthalpies at different heating rates.

IV. CONCLUSION

For the kinetics study on thermal–oxidative decomposition of CIGS with chalcopyrite structure in air, there are two stages of thermal–oxidative decomposition, namely CIGS with chalcopyrite structure decomposing into binary/ternary selenide, and binary/ternary selenide oxidizing into oxide. In Stage I and Stage II thermal–oxidative decompositions, the invariant kinetic parameters apparent activation energy are 143.76 and 222.81 kJ/mol, respectively, and the frequency factor 20.93 and 25.90 1/sec, respectively; the synthesis conversion mode functions for both stages of thermal–oxidative decomposition are the same $g(\alpha)=(1-\alpha)^{-2}-1$, which indicates that both the two stages of the thermal–oxidative decomposition of CIGS with chalcopyrite structure are the random nucleation of three epipoles on one. Separate particle.

TABLE 3
SUMMARY OF ACTIVATION THERMODYNAMIC PARAMETERS FOR THERMAL–OXIDATIVE DECOMPOSITION OF CIGS WITH CHALCOPYRITE STRUCTURE

	Rh (°C/min)	2	5	10	Avg.
First tage	$\Delta G \neq$ (kJ/mol)	190.53	192.30	193.65	192.16
	$\Delta H \neq$ (kJ/mol)	138.70	138.53	138.40	138.54
	$\Delta S \neq$ (kJ/K·mol)	-0.085	-0.085	-0.086	-0.085
Second stage	$\Delta G \neq$ (kJ/mol)	253.03	254.04	254.83	253.97
	$\Delta H \neq$ (kJ/mol)	216.16	216.00	215.84	215.99
	$\Delta S \neq$ (kJ/K·mol)	-0.046	-0.046	-0.046	-0.046

REFERENCES

[1] S. Ahn, C. Kim, J. Yun, J. Lee, and K. Yoon, "Effects of heat treatments on the properties of Cu (In, Ga) Se2 nanoparticles," *Solar Energy Materials and Solar Cells*, vol. 91, no. 19, pp. 1836–1841, 2007. doi: https://doi.org/10.1016/j.solmat.2007.06.014

[2] M. A. Greeny, K. Emery, Y. Hishikawa, and W. Warta, "Solar cell efficiency tables (version 37)," *Progress in Photovoltaics*, vol. 19, no. 1, pp. 84–92, 2011.

[3] K. Ramanathan, M. A. Contreras, C. L. Perkins, S. Asher, F. S. Hasoon, J. Keane, D. Young, M. Romero, W. Metzger, R. Noufi *et al.*, "Properties of 19.2% efficiency ZnO/CdS/CuInGaSe2 thin-film solar cells," *Progress in Photovoltaics: Research and Applications*, vol. 11, no. 4, pp. 225–230, 2003. doi: https://doi.org/10.1002/pip.494

[4] I. Repins, M. A. Contreras, B. Egaas, C. DeHart, J. Scharf, C. L. Perkins, B. To, and R. Noufi, "19· 9%-efficient ZnO/CdS/CuInGaSe2 solar cell with 81· 2% fill factor," *Progress in Photovoltaics: Research and applications*, vol. 16, no. 3, pp. 235–239, 2008. doi: https://doi.org/10.1002/pip.822

[5] Y.-H. Li, *Thermal Analysis*. Hsinchu, Taiwan: National Tsing Hua University, 1978.

[6] Z. Xu, C. Shen, Y. Hou, H. Gao, and S. Sun, "Oleylamine as both reducing agent and stabilizer in a facile synthesis of magnetite nanoparticles," *Chemistry of Materials*, vol. 21, no. 9, pp. 1778–1780, 2009. doi: https://doi.org/10.1021/cm802978z

[7] J. P. Elder, "Thee-ln (a)-f (α)'triplet in non-isothermal reaction kinetics analysis," *Thermochimica Acta*, vol. 318, no. 1-2, pp. 229–238, 1998. doi: https://doi.org/10.1016/S0040-6031(98)00347-5

[8] D. Trache, A. Abdelaziz, and B. Siouani, "A simple and linear isoconversional method to determine the pre-exponential factors and the mathematical reaction mechanism functions," *Journal of Thermal Analysis and Calorimetry*, vol. 128, no. 1, pp. 335–348, 2017. doi: https://doi.org/10.1007/s10973-016-5962-0

[9] P. Gallagher and D. Johnson Jr, "Kinetics of the ther-

mal decomposition of CaCO_3 in CO_2 and some observations on the kinetic compensation effect," *Thermochimica Acta*, vol. 14, no. 3, pp. 255–261, 1976. doi: https://doi.org/10.1016/0040-6031(76)85002-2

[10] G. Manikandan, G. Rajarajan, J. Jayabharathi, and V. Thanikachalam, "Structural effects and thermal decomposition kinetics of chalcones under non-isothermal conditions," *Arabian Journal of Chemistry*, vol. 9, pp. 570–575, 2016. doi: https://doi.org/10.1016/j.arabjc.2011.06.029

[11] L. Xia, L. Zuo, X. Wang, D. Lu, and R. Guan, "Non-isothermal kinetics of thermal degradation of DGEBA/TU-DETA epoxy system," *Journal of Adhesion Science and Technology*, vol. 28, no. 18, pp. 1792–1807, 2014. doi: https://doi.org/10.1080/01694243.2014.922454

[12] L. Shi and D. Northwood, "A note on ostwald ripening kinetics and reaction rate theory," *Physica Status Solidi (a)*, vol. 133, no. 1, pp. 1–5, 1992. doi: https://doi.org/10.1002/pssa.2211330119

[13] J. Zhang, Z. Lin, Y. Lan, G. Ren, D. Chen, F. Huang, and M. Hong, "A multistep oriented attachment kinetics: Coarsening of ZnS nanoparticle in concentrated NaOH," *Journal of the American Chemical Society*, vol. 128, no. 39, pp. 12 981–12 987, 2006. doi: https://doi.org/10.1021/ja062572a